Computational Study on the Photophysics of Protonated Benzene

Michal F. Rode,[†] Andrzej L. Sobolewski,[†] Claude Dedonder,[‡] Christophe Jouvet,[‡] and Otto Dopfer*[,§]

Institute of Physics, Polish Academy of Sciences, PL-02668 Warsaw, Poland, Laboratoire de Photophysique Moléculaire du CNRS, Bat. 210, Université Paris-Sud, F-91405 Orsay Cedex, France, and Institut für Optik and Atomare Physik, Technische Universität Berlin, Hardenbergstrasse 36, D-10623 Berlin, Germany

Received: March 26, 2009

The reaction paths in the lowest excited electronic states relevant for the photophysics of protonated benzene, $C_6H_7^+$, have been explored by ab initio techniques of electronic structure theory. For this purpose, the first four excited singlet electronic states of $C_6H_7^+$ have been calculated at the CC2/cc-pVTZ level of theory. The CC2 approach has been validated by CASPT2 and TD-DFT calculations. The calculated UV absorption spectrum is in good agreement with the experimental spectrum. It has been found that the out-of-plane and the in-plane ring deformation leads in the excited states in an essential barrierless manner to a low-lying conical intersection between the lowest excited states and with the ground state, providing a mechanism for efficient radiationless deactivation, which is expected to quench luminescence of the isolated molecular ion.

1. Introduction

Protonated aromatic hydrocarbon molecules, in the following denoted AH^+, constitute a fundamental class of organic molecules. They occur as short-lived intermediates in a broad range of environments, ranging from astrochemistry, jet engine gas exhaust,[1] and organic chemistry to biophysics. For example, AH^+ are widely accepted as intermediates in electrophilic aromatic substitution reactions (σ complexes),[2] the most important reaction mechanism of aromatic molecules.[3] In addition, AH^+ ions have been detected in various hydrocarbon plasmas (e.g., flame combustion).[4] They are also invoked to be present in interstellar space and are considered as candidates for the carriers of the unidentified IR emission bands observed in various interstellar media.[5−7] In addition, the effect of protonation of aromatic biomolecular building blocks is an interesting issue for models rationalizing the UV photostability of biological macromolecules, such as proteins and DNA.[8−10]

Despite their importance, and quite surprisingly, until recently[11] very little has been known experimentally[12,13] about the geometric and electronic structure as well as the dynamics of even simple isolated AH^+ ions, mainly because of the difficulties encountered in the production of high concentrations of these reactive species in the gas phase, which are required to probe their properties by spectroscopy. Recent advances in the development of efficient ion sources and sensitive IR spectroscopic detection and ion trapping techniques have allowed substantial progress in the characterization of the geometric structure of isolated and microsolvated AH^+ ions in the gas phase.[7,9,11,14−19]

The main recent advances in the knowledge of gas-phase AH^+ ions are briefly reviewed. The coupling of a supersonic expansion with an octopole ion trap and an IR optical parametric oscillator laser has been utilized to obtain the first high-resolution spectra of gas-phase AH^+ ions, such as protonated benzene and phenol, which provided spectroscopic information about the preferred protonation site in their ground electronic states.[7,11,15−17,20−22] Similar structural information on a variety of fundamental AH^+ ions has recently been obtained by combining an intense IR free electron laser with ion trapping techniques, utilizing multiple photon dissociation spectroscopy in the IR fingerprint range.[6,23−28] The development of a cold 22-pole ion trap has permitted the capture of AH^+ ions at low temperatures (5 K).[29−31] This device coupled with IR and UV nanosecond lasers has enabled the first spectroscopic characterization of the more stable structures of protonated aromatic amino acids and their fragmentation after electronic excitation. In particular, it has been shown that protonated tyrosine has a well-structured excited state, whereas protonated tryptophan displays a very broad band implying a very short lifetime of the excited state.[9] The coupling of an electrospray ion source with a pump−probe femtosecond laser yielded for the first time direct information on the excited-state lifetimes of protonated aromatic amino acids (tryptophan ∼400 fs, tyrosine ∼15 ps),[32−34] which are in agreement with the spectroscopic analysis.[9] The coupling of this source with a coincidence experiment, detecting in time and in position all ions and neutrals issued from photofragmentation, has allowed for the first time a complete analysis of the fragmentation process of these ions (pathways and time scales).[35,36] From a theoretical point of view, the recent possibility of performing optimizations of excited states at electron-correlated ab initio levels (e.g., RI-CC2 as implemented in the TURBOMOLE program package)[37] has allowed a reliable comparison to be made with experimental data resulting in a deeper understanding of the relaxation and fragmentation dynamics observed after electronic excitation.[38−40]

In this paper, we present results of ab initio calculations on the photophysical properties of the most fundamental protonated aromatic molecule, namely, protonated benzene ($C_6H_7^+$). Previous quantum chemical calculations agree that the benzenium ion (σ complex, C_{2v} symmetry) is the global minimum on the potential energy surface in the ground electronic state of $C_6H_7^+$ (Figure 1a).[11,41−43] The bridged structure (benzonium, C_s symmetry) corresponds to a transition state between equivalent σ complexes, with an activation barrier of around 0.25−0.45 eV for proton migration. The π complex (C_{6v} symmetry) is identified as a high-

* Corresponding author, dopfer@physik.tu-berlin.de.
[†] Institute of Physics, Polish Academy of Sciences.
[‡] Laboratoire de Photophysique Moléculaire du CNRS, Bat. 210, Université Paris-Sud.
[§] Institut für Optik and Atomare Physik, Technische Universität Berlin.

10.1021/jp902729m CCC: $40.75
Published on Web 04/29/2009

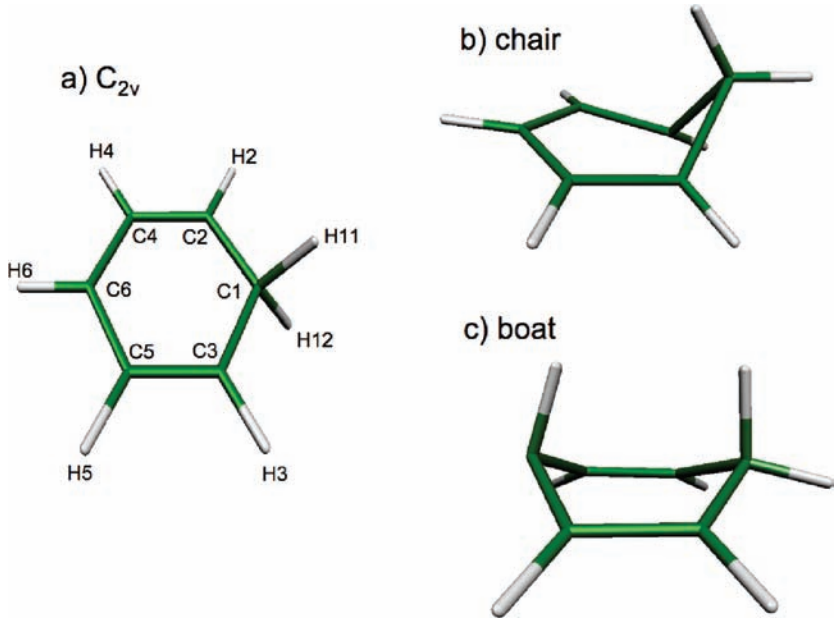

Figure 1. Selected structures of protonated benzene ($C_6H_7^+$). (a) Ground state (S_0) geometry obtained at the MP2/cc-pVTZ level (Table 1) denoted *C_{2v} structure*, along with the numbering of the atoms. (b) Minimum structure of the 1A″ ($1B_2$) state (S_1) obtained at the CC2/cc-pVTZ level (Table 3) denoted *chair*. (c) Minimum structure of the first excited 2A′ ($2A_1$) state (S_3) obtained at the CC2/cc-pVTZ level (Table 3) denoted *boat*.

lying saddle point lying roughly 2 eV above the σ complex. Condensed phase spectroscopic (NMR, IR, UV)[44−50] and crystallographic data[48,49] of $C_6H_7^+$ in salts or superacid solutions are consistent with these theoretical predictions. Recent IR spectroscopic work of isolated $C_6H_7^+$ and its microsolvated clusters, $C_6H_7^+-L_n$ (L = Ar, N_2, CH_4, H_2O),[5,11,16,17,20,23] confirmed that the σ complex is also the most stable structure of $C_6H_7^+$ in the gas phase. Interestingly, the gas-phase IR spectrum closely resembled that in the condensed phase, implying that the structure is relatively little perturbed in the bulk.[7] The only information about the electronically excited states of $C_6H_7^+$ is available from early UV absorption spectra in solution[50] and a low-resolution UV photodissociation spectrum of $C_6H_7^+$ isolated in a Fourier transform ion cyclotron resonance mass spectrometer.[12,13] The gas-phase spectrum revealed two transitions at 330 and 245 nm and deviates significantly from the solution spectrum.[12,13] No firm interpretation for the assignment of the transitions observed has been offered so far. Preliminary interpretations given in ref 12 rely on early quantum chemical approaches, which tentatively correlate the 330 and 245 nm bands with transitions from the $^1A_1$ ground state into the $^1B_2$ and $^1A_1$ excited states, respectively.[52,53] As, to the best of our knowledge, high-level ab initio calculations of electronically excited states of $C_6H_7^+$ have not been reported so far, the present work offers the first attempt at a reliable assignment of the UV spectrum of this fundamental arenium ion.

2. Computational Methods

As protonated benzene, $C_6H_7^+$, has a closed-shell singlet electronic ground state, the MP2 method appears appropriate to characterize the ground electronic state, since this technique usually yields accurate geometries for closed-shell molecules.[54] Previously, also DFT methods were employed to investigate the related polyene cations[55,56] in their singlet ground electronic states and it was found that, especially for odd-numbered polyene cations such as $C_{13}H_{15}^+$, both MP2 and hybrid-DFT methods provide satisfactory results for the ground-state geometry. Moreover, it was observed that the time-dependent DFT (TD-DFT) technique yields much more reliable excitation energies for polyene cations than for neutral polyenes,[55,56] leading to good agreement with high-level ab initio calculations and experimental results. For this reason, the excited states of $C_6H_7^+$ are characterized in the present work by ab initio methods, namely, CC2 and CASPT2 (multireference complete active space second-order perturbation theory), and complementary TD-DTF calculations.

Ab initio calculations for $C_6H_7^+$ have been performed with the TURBOMOLE program package,[37] making use of the resolution-of-the-identity (RI) approximation for the evaluation

TABLE 1: CC2/cc-pVDZ Optimized Geometric Parameters of the Local Minima of the First Four Excited States in C_{2v} Symmetry Compared to the MP2/cc-pVDZ Optimized S_0 Equilibrium Structure

	$S_0(1A_1)$	$S_1(1B_2)$	$S_2(1A_2)$	$S_3(2A_1)$	$S_4(1B_1)$
			Distances/Å		
C2−C3	2.516	2.462	2.422	2.552	2.717
C4−C5	2.491	2.458	2.407	2.520	2.462
C1−C2	1.470	1.496	1.558	1.485	1.533
C2−C4	1.385	1.416	1.344	1.436	1.393
C4−C6	1.417	1.448	1.441	1.455	1.418
H11−C1	1.117	1.117	1.106	1.126	1.120
H12−C1	1.117	1.117	1.106	1.126	1.120
H6−C6	1.097	1.092	1.091	1.095	1.098
C1−C6	2.823	3.03	3.112	2.923	2.802
			Angles/deg		
C2−C1−C3	117.6	110.8	102.0	118.5	124.8
C1−C2−C4	120.7	124.5	128.7	120.1	112.4
C2−C4−C6	119.0	122.0	123.7	120.7	125.0
C4−C6−C5	123.0	116.2	113.3	120.0	120.5
H11−C1−H12	100.3	102.5	109.2	97.7	123.5
H6−C6−C4	118.5	121.9	123.4	120.0	120.0
			Dihedral Angles/deg		
H6−C6−C4−C2	180.0	180.0	180.0	180.0	180.0
C6−C4−C2−C3	0.0	0.0	0.0	0.0	0.0
C1−C2−C4−C5	0.0	0.0	0.0	0.0	0.0
			Energies/eV		
$E(S_0)^a$	0.000	0.236	1.039	0.189	0.867

[a] Energy of the S_0 state relative to the energy of its equilibrium structure.

of the electron-repulsion integrals.[57] The equilibrium geometry of $C_6H_7^+$ in its closed-shell singlet ground electronic state (S_0) has been determined with the MP2[58] and DFT methods.[59,60] Excitation energies and response properties have been calculated with the CC2 method[61,62] at the geometry optimized at the MP2 level. The equilibrium geometries of the lowest excited singlet states (S_1-S_4) have been determined at the CC2 level, making use of the recently implemented CC2 analytic gradients,[63] and at the TD-DFT[64] level for comparison. The minimum energy paths along the photophysically relevant reaction coordinates in the lowest excited singlet states have also been determined with the CC2 method. For comparison, vertical excitation energies have also been obtained using the CASPT2[65,66] and TD-DFT techniques at the geometry optimized at the MP2 level. The adiabatic energies obtained at the CC2 level were also compared to CASPT2 results calculated at the geometries of the excited state optimized at the CC2 level and to TD-DFT results derived at excited-state geometries optimized at the TD-DFT level. The CASPT2 calculation was performed with the software package MOLPRO.[67] This calculation was based on a CASSCF active space of 14 electrons in 12 orbitals ($3a_1$, $3b_2$, $4b_1$, $2a_2$).[68] This active space includes 4σ and 3π valence orbitals as well as $2\sigma^*$ and $3\pi^*$ virtual orbitals. The state-averaged CASSCF technique was used, and two states of A_1 symmetry and one state of A_2, B_1, and B_2 symmetry were taken into account. To avoid intruder state problems, a level shift of 0.3 was used in the CASPT2 calculation. Such a methodology using the CASPT2 and CC2 methods has well reproduced experimental values of vertical and adiabatic excitation energies in related systems.[69] In the case of the TD-DFT calculation, the B3-LYP[70] hybrid density functional was employed.

Closer inspection of the geometries optimized in the excited states enabled us to identify certain coordinates, which can drive the relaxation process from the initially excited state to the ground state. Once the choice of the relevant coordinate was made, the energy path has been calculated following this driving coordinate, and all other nuclear degrees of freedom have been optimized for a given value of this coordinate. Throughout these calculations, the correlation-consistent polarized valence double-ζ (cc-pVDZ) basis set[71] has been employed. The same basis set was used in the calculation of the final vertical excitation energies and oscillator strengths at the optimized geometries. These calculations were additionally performed with the use of the triple-ζ (cc-pVTZ) basis set[71] in order to evaluate the effect of the size of the basis set on the calculated quantities. The search for conical intersection geometries has been performed employing the Gaussian03 program package,[72] by use of the state-averaged CASSCF method with the active space comprising of six electrons in six orbitals. In this calculation, two states of C_1 symmetry were taken into account and the cc-pVDZ basis set was used.

3. Results and Discussion

3.1. Ground State Equilibrium Structure of $C_6H_7^+$. In agreement with previous calculations,[11,41-43] the equilibrium structure of $C_6H_7^+$ in its A_1 ground electronic state, S_0, has C_{2v} symmetry (σ complex). The structure is planar with the exception of the CH_2 group (C1−H11−H12), which lies in a plane perpendicular to the plane of the benzene ring (Figure 1a). This structure is the only minimum located on the S_0 potential and will hereafter be referred to as the *C_{2v} structure*.

Table 1 summarizes the relevant geometric parameters of $C_6H_7^+$ evaluated at the MP2/cc-pVDZ level. For comparison, the geometry obtained at the DFT level is given in the Supporting Information. In general, the MP2 level gives slightly longer C−C distances but the differences are smaller than 0.01 Å. Both C−H covalent bonds in the aliphatic CH_2 moiety are slightly elongated (1.117 Å) as compared to the corresponding aromatic C−H bonds in the isolated benzene molecule (1.095 Å). The CH_2 bond angle amounts to 100.3° for the minimum. Nonetheless, all the C−C−C bond angles are more or less around 120°, suggesting that the aromatic character of the molecule is largely maintained. Nethertheless, protonation at the C1 atom elongates the C1−C2 distance to 1.470 Å from the corresponding aromatic C−C bonds in the isolated benzene molecule (1.407 Å). The C2−C4 and most distant C4−C6 bonds are less affected, with distances of 1.385 and 1.417 Å, respectively. The degree of the structural perturbation of the benzene ring induced by protonation is also visible in the bond length alternation (BLA) parameter, which is defined as the difference between alternating single (C−C) and double or triple (C═C, C≡C) bond distances and usually used in the context of conducting polymers, such as polyacetylene. The BLA parameter for closed-shell neutral polyenes was determined as 0.068 Å at the MP2 level and 0.071 Å at the hybrid DFT level.[55] For closed-shell odd-numbered polyene cations, the BLA parameter even reaches values up to 0.073 (MP2) and 0.081 Å (DFT) in the case of $C_{13}H_{15}^+$ at the chain ends.[55] For protonated benzene, the BLA parameter amounts to 0.085 Å (MP2) for the difference between the C1−C2 and C2−C4 bond distances (a value comparable to that of odd-numbered polyene cations or neutral polyenes) and to 0.053 Å (MP2) for the difference between the C1−C2 and C4−C6 bond distances. The DFT method yields slightly larger values of 0.096 and 0.056 Å, respectively, implying that the MP2 geometry of protonated benzene in its ground electronic state is slightly more aromatic than the DFT geometry in terms of bond length alternation.

TABLE 2: Vertical Excitation Energies (ΔE), Oscillator Strengths (f), and Dominant Electronic Configurations of the Lowest Excited Singlet States of $C_6H_7^+$ Calculated with the CC2/cc-pVTZ Method at the Ground-State Equilibrium Geometry Obtained at the MP2/cc-pVTZ level (*C_{2v} structure*)

state	ΔE/eV[a]	f	orbital configuration
S_0, $1A_1$	0.0		
S_1, $1B_2(\pi\pi^*)$	4.094 (4.069)	0.14313	$0.98(1a_2-3b_1)$
S_2, $1A_2(\sigma\pi^*)$	5.514 (5.522)	0.0000	$0.99(7b_2-3b_1)$
S_3, $2A_1(\pi\pi^*)$	5.709 (5.674)	0.0956	$0.90(2b_1-3b_1) - 0.41(1a_2-2a_2)$
S_4, $1B_1(\sigma\pi^*)$	5.716 (5.714)	0.00498	$0.98(11a_1-3b_1)$

[a] Values in parentheses are obtained at the CC2/cc-pVDZ level.

3.2. Vertical Absorption Spectrum of $C_6H_7^+$. Vertical excitation energies of the ground-state equilibrium structure of $C_6H_7^+$ calculated at the CC2/cc-pVTZ level are listed in Table 2. The molecular orbital configuration in the ground electronic state with A_1 symmetry (denoted $1A_1$ state) can be described as...$(10a_1)^2(11a_1)^2(7b_2)^2(2b_1)^2(1a_2)^2(3b_1)^0(2a_2)^0$..., and Figure 2 illustrates the shape of the relevant molecular orbitals evaluated at the HF/cc-pVTZ level. The occupied $10a_1$, $11a_1$, and $7b_2$ orbitals have σ character, whereas the two highest occupied ($2b_1$, $1a_2$) and the two lowest unoccupied ($3b_1$, $2a_2$) orbitals have π and π^* character, respectively. The lowest excited singlet state (S_1) of $C_6H_7^+$ results from the excitation from the HOMO orbital ($1a_2$) to the LUMO orbital ($3b_1$), giving a $\pi\pi^*$ orbital character to this state of B_2 symmetry. The first optically allowed transition ($1B_2-1A_1$) occurs at a vertical excitation energy of 4.094 eV, with a significant oscillator strength of $f = 0.143$ (Table 2). The next excited state, S_2, has A_2 symmetry and $\sigma\pi^*$ orbital character, because it results from excitation from the

TABLE 3: CC2/cc-pVDZ Optimized Geometric Parameters of the Local Minima of the Excited States in C_s Symmetry, Compared to the MP2/cc-pVDZ Optimized S_0 Equilibrium Structure

	C_{2v} structure $S_0(1A')$	chair(1) $S_1(1A'')$	chair(2) $S_1(1A'')^a$	boat $S_3(1A')$
	Distances/Å			
C2−C3	2.516	2.099	1.970	2.572
C4−C5	2.491	2.410	2.364	2.566
C1−C2	1.470	1.505	1.494	1.502
C2−C4	1.385	1.429	1.430	1.398
C4−C6	1.417	1.431	1.417	1.468
H11−C1	1.117	1.102	1.084	1.137
H12−C1	1.117	1.096	1.082	1.100
H6−C6	1.097	1.094	1.078	1.125
C1−C6	2.823	2.897	2.905	2.617
	Angles/deg			
C2−C1−C3	117.6	88.5	82.5	117.8
C1−C2−C4	120.7	118.6	118.9	117.9
C2−C4−C6	119.0	115.9	115.2	110.3
C4−C6−C5	123.0	114.9	113.1	121.8
H11−C1−H12	100.3	114.3	114.4	105.6
H6−C6−C4	118.5	122.3	123.0	102.7
	Dihedral Angles/deg			
H6−C6−C4−C2	180.0	178.3	178.2	65.4
C6−C4−C2−C3	0.0	5.1	5.4	21.4
C1−C2−C4−C5	0.0	−42.3	−46.8	−14.0
	Energies/eV			
$E(S_0)^b$	0.000	3.109	2.644	4.334

[a] Calculation at the CASSCF(6,6) level. [b] Energy of the S_0 state relative to the energy of its equilibrium structure.

$7b_2$ to the $3b_1$ orbital. Its energy is 5.514 eV, almost 1.5 eV above the $S_1(1B_2)$ state. The S_2-S_0 transition is optically dipole forbidden, but it may borrow intensity through vibronic coupling from the two nearby states lying just 0.2 eV above. These states, $S_3(2A_1)$ and $S_4(1B_1)$, are almost degenerate (5.709 and 5.716 eV) and absorb moderately ($f = 0.0956$ and 0.00498). The $S_3(2A_1)$ state is of $\pi\pi^*$ and the $S_4(1B_1)$ state is of $\sigma\pi^*$ orbital character, because they arise from excitation from $2b_1$ and $11a_1$ into the LUMO ($3b_1$), respectively. These three excited states, $S_2(1A_2)$, $S_3(2A_1)$, and $S_4(1B_1)$, lie in a narrow energy range between 5.514 and 5.716 eV above the ground state. As the S_5 and S_6 states occur at much higher energies (7.56 and 7.68 eV), they are not considered further. In general, the energy values obtained at the CC2/cc-pVTZ level are close to those at the CC2/cc-pVDZ level, with a maximum deviation of 0.035 eV (Table 2), suggesting that the latter level is sufficiently accurate for further quantum chemical investigations. Additional comparison of the vertical excitation energies evaluated at various theoretical levels (CC2, CASPT2, TD-DFT) employing the cc-pVTZ basis set is given in Table S1 in Supporting Information, yielding the following major conclusions. Both the single-reference CC2 and the multireference CASPT2 level of theory yield the same ordering of the excited states at the Franck−Condon region. In particular, the lowest excited state, $S_1(B_2)$, is significantly lower in energy than the three other excited states considered. Moreover, the CASPT2 excitation energies are for each state consistently lower than the corresponding CC2 values by approximately 0.7 eV. Since it is known[73] that the CC2 method overestimates the excitation energies by ca. 0.3 eV, the expected excitation values for each state may be lying somewhere between the CC2 and CASPT2 results. The TD-DFT results shown in Table S1 of the Supporting Information indeed support this hypothesis.

In order to compare with the experiment,[12,13] the simulated UV absorption spectrum is presented in Figure 3b, assuming vertical transition energies at the equilibrium geometry of the ground state, the corresponding oscillator strengths (Table 2), and a convolution of the stick spectra with a Gaussian function of 0.5 eV full width at half maximum. The spectrum reveals two distinct absorption bands. The lower-energy band is related to the absorption into the $S_1(1B_2)$ electronic state. The profile of the higher-energy band results from the overlapping absorptions into the $S_3(2A_1)$ and $S_4(1B_1)$ states.

3.3. Excited-State Equilibrium Structures and Relaxation Mechanisms. Optimization of the geometry of an electronically excited state (with respect only to its own energy) is generally only possible if the close-lying states belong to different orbital symmetry. Our preliminary attempt to excited-state geometry optimization has led us to the conclusion that the lowest excited singlet states of $C_6H_7^+$ have minima, which conserve either C_{2v} or C_s symmetry.

In C_s symmetry, with the mirror plane containing the CH_2 group and the C6−H6 bond, the two lowest excited states with B_2 and A_2 symmetry in the C_{2v} point group correlate to the A″ irreducible representation, whereas the next two excited states, A_1 and B_1, belong to the A′ irreducible representation. To omit further ambiguity due to the reduction of the symmetry from C_{2v} to C_s upon relaxation of the geometry, the $1B_2$ and $1A_2$ states will be abbreviated 1A″ and 2A″, respectively. These states will be hereafter denoted as S_1 and S_2 electronic states, respectively. Similarly, the $2A_1$ and $1B_1$ states correlating to 2A′ and 3A′ in C_s symmetry, will be denoted below as S_3 and S_4 states, respectively. In this notation, the ground state, $S_0(1A_1)$, correlates to 1A′.

The overall energy scheme and the relaxation mechanisms of the first excited states leading to conical intersections with the lower excited states and the ground state without any barrier are summarized in Figure 4 (CC2/cc-pVDZ level). The rest of this section is devoted to a discussion of the possible relaxation mechanisms of the first four excited singlet electronic states, S_1-S_4.

The calculation of the adiabatic excitation energies (ΔE_a) were conducted for the excited-state minimum geometries optimized in C_{2v} symmetry, since only these geometries are close to the Franck−Condon region. The results of the vertical (ΔE_v) and adiabatic (ΔE_a) excitation energies obtained at different theoretical levels (CC2, CASPT2, TD-DFT) are compared in Table S2 in the Supporting Information.

3.3.1. Relaxation Mechanism of the $S_1(\pi\pi^*)$ Electronic State. Optimization of the lowest excited $S_1(1B_2)$ state under C_{2v} symmetry constraint starting from the vertical Franck−Condon region lowers its energy by 0.25 eV (see Table S2 in Supporting Information, CC2/cc-pVDZ level). It is a relatively small gain in energy observed upon minimization within the C_{2v} symmetry constraint. The energy gain upon relaxation of the three other states amounts to 0.88, 0.21, and 0.49 eV for $S_2(1A_2)$, $S_3(2A_1)$, and $S_4(1B_1)$, respectively. The small stabilization energy gained in optimizing the $S_1(\pi\pi^*)$ state is linked to minor geometry changes. This in turn implies also only a modest increase in the ground state (S_0) energy of 0.24 eV for this geometry (similar to the $S_3(\pi\pi^*)$ state). As a net result, the energy gap between S_1 and S_0 decreases from 4.07 to 3.82 eV, when moving from the S_0 optimal structure to the S_1 optimal geometry. As this energy change is small compared to the vertical S_0-S_1

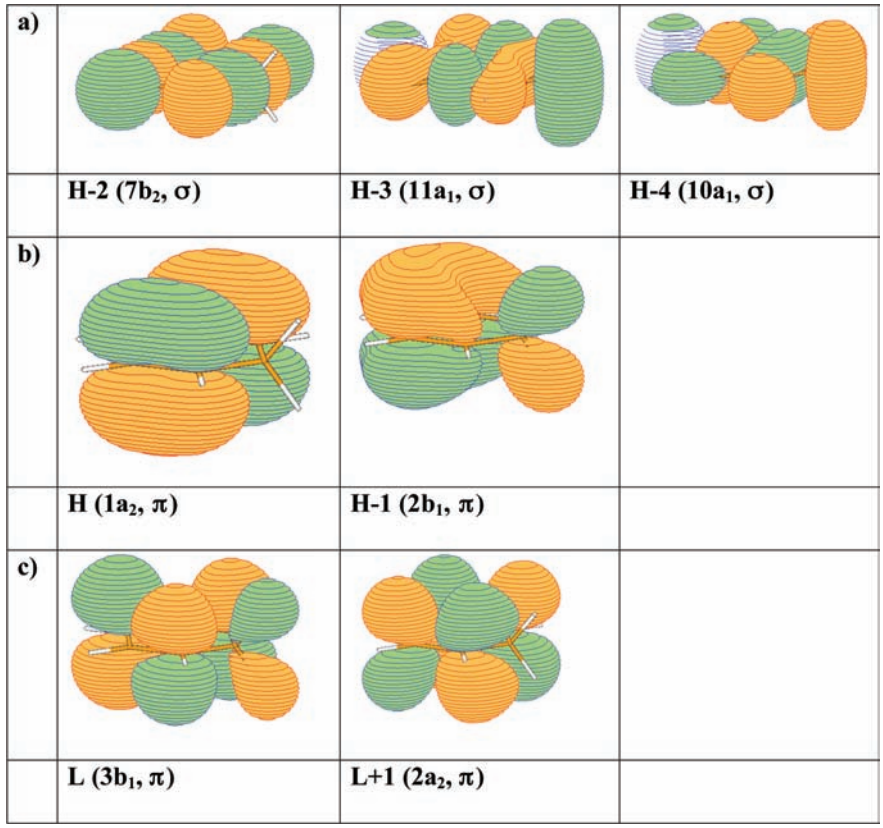

Figure 2. The highest three occupied orbitals with σ character, H-2, H-3, H-4 (a), the highest two occupied π orbitals, H and H-1 (b), and the lowest two unoccupied π orbitals, L and L + 1 (c), determined for the equilibrium geometry of the electronic ground state (S_0) of $C_6H_7^+$ at the HF/cc-pVTZ level. H and L indicate HOMO and LUMO, respectively.

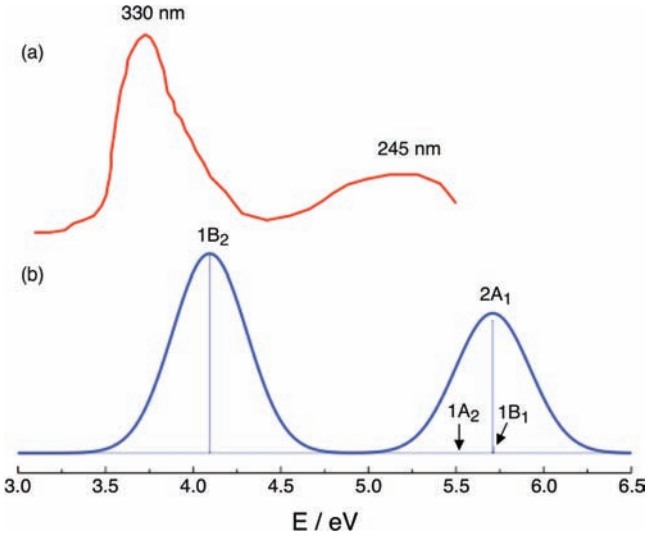

Figure 3. (a) Experimental UV photodissociation spectrum of $C_6H_7^+$ (adapted from ref 13). (b) Simulated UV absorption spectrum assuming vertical transition energies at the equilibrium geometry of the S_0 state, the corresponding oscillator strengths (Table 1), and a convolution of the stick spectra with a Gaussian function of 0.5 eV full width at half-maximum.

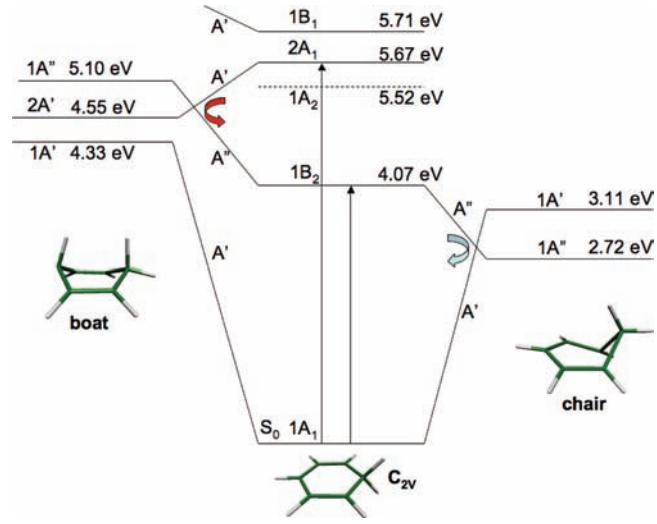

Figure 4. Energy level diagram of the five lowest singlet states of $C_6H_7^+$ at three selected geometries evaluated at the CC2/cc-pVDZ level (Tables 2 and 3): vertical excitation energies at the ground-state equilibrium geometry (central part, C_{2v} symmetry); energies of the states at the optimized geometry of the first 1A″ excited state (right part, C_s symmetry); energies of the states at the optimized geometry of the first 2A′ excited state (left part, C_s symmetry).

transition energy, the molecular ion will have to undergo more profound geometrical changes to reduce the gap between these two states to reach an eventual conical intersection region.

When the symmetry is reduced from C_{2v} to C_s, the optimization of the $S_1(1B_2)$ state (turning into the 1A″ state) leads to a substantial out-of-plane deformation of the benzene ring. Indeed the $S_1(1B_2)$ state, being of $\pi\pi^*$ orbital character, is unstable with respect to such an out-of-plane deformation of the benzene ring,[74−76] and the unconstrained energy optimization leads without any barrier to the chairlike structure shown in Figure 1b and labeled chair(1) in Table 3 (for simplicity, we denote this half-chair type structure chairlike in the present work). The distinct feature of this structure is the out-of-plane movement of the CH_2 group. The corresponding minimum energy path of this state, driving the system to the S_1/S_0 conical intersection

region, is shown in Figure S1 in the Supporting Information. Along this reaction path, the interatomic C2−C3 distance decreases from 2.516 to 2.099 Å, whereas the C4−C5 separation decreases from 2.491 to 2.410 Å. In addition, the benzene ring bond angles are deformed. The total stabilization energy of the $S_1(1A'')$ state after the unconstraint optimization amounts to 1.35 eV with respect to the vertical (Franck−Condon) energy of 4.07 eV, leading to an energy of 2.72 eV (see Figure 4, right part). With the same chair(1) geometry, the energy of the $S_0(1A')$ ground-state substantially increases up to 3.11 eV. Thus, the first 1A″ state becomes lower in energy than the first 1A′ state in the chair(1) geometry. This energetics suggest that the chair(1) structure is a good candidate for a conical intersection point between the S_0 and S_1 electronic states. Let us mention in this context that this reaction path is qualitatively similar to these previously computed for benzene and pyrazine.[77,76]

Since the CC2 method fails at conical intersections, we have employed the CASSCF method to locate the conical intersection point. The resulting chair(2) structure has indeed similar geometric parameters as chair(1) (Table 3). When a CC2 calculation of the vertical excitation energies is performed with the chair(2) structure, a small energy gap between S_0 and S_1 of 0.35 eV is also obtained, S_0 and S_1 being located at 2.64 and 2.79 eV above the ground equilibrium geometry. Thus, we have identified a barrierless pathway leading from the Franck−Condon region of the first excited state to a conical intersection with the ground state. As a consequence, the energy of the photo-excited $S_1(1B_2)$ state is expected to be dissipated radiationless into heat through a conical intersection on the femtosecond time scale, via out-of-plane deformations.

3.3.2. Relaxation Mechanism of the $S_2(\sigma\pi^*)$ Electronic State. The S_2-S_0 transition is optically forbidden, but the S_2 state may be populated via relaxation processes from higher-lying optically bright states, such as the $S_3(2A_1)$ and $S_4(1B_1)$ states. The $\sigma\pi^*$ orbital character of the $S_2(1A_2)$ state tends to stabilize planar structures, in a similar way as the $\sigma\pi^*$ orbital character stabilizes the planar excited states of pyridine and pyrazine.[75,78] To demonstrate this effect, we have optimized the S_2 state starting from a slightly out-of-plane distorted geometry (2A″ state in C_s symmetry). The optimized minimum-energy structure is indeed planar and corresponds to the same structure as optimized under C_{2v} symmetry constraint. The relaxation energy from the Franck−Condon region amounts to 0.88 eV, and the major geometry changes are a contraction of the C2−C3 and C4−C5 interatomic distances of almost 0.1 Å and a decrease of the C2−C1−C3 bond angle to 102°. The fact that the optimal geometry of the S_2 state is planar allows us to presume that an eventual S_2/S_1 conical intersection should be found in C_{2v} symmetry. Indeed, the energies of the $S_2(1A_2)$, $S_1(1B_2)$, and $S_0(1A_1)$ states at this geometry are 4.65, 4.54, and 1.04 eV above the ground-state equilibrium geometry, respectively, implying a small S_2-S_1 energy gap of the order of only 0.1 eV indicative of a conical intersection.

3.3.3. Relaxation Mechanism of the $S_3(\pi\pi^*)$ and $S_4(\sigma\pi^*)$ States. The second absorption band in the UV spectrum in Figure 3b arises from transitions into two almost degenerate, optically allowed states, $S_3(2A_1)$ and $S_4(1B_1)$, which arise from two different types of electronic excitations. The $S_3(2A_1)$ state has $\pi\pi^*$ character, whereas the $S_4(1B_1)$ state is a result of $\sigma\pi^*$ excitation. As a consequence, the $S_4(1B_1)$ state, which can directly be populated by vertical excitation from the S_0 state, will tend to relax to its optimal geometry in C_{2v} symmetry. On the other hand, relaxation of the $S_3(2A_1)$ state, which is the first excited A′ state in C_s symmetry, will tend to break the C_{2v} symmetry and is expected to cross the second A″ state, $S_2(1A_2)$, which will pull the geometry relaxation process back to a planar structure with C_{2v} symmetry (Figure 4).

Indeed, when the C_{2v} constraint is released, optimization of the $S_3(2A')$ state ends up at a boatlike structure presented in Figure 1c and its geometric parameters are given in Table 3. This relaxation process involves a simultaneous out-of-plane distortion of the CH and CH_2 groups at the two opposite ends of protonated benzene. Moreover, the C6−H6 valence bond, pointing toward one of the protons of the CH_2 moiety in the resulting boat structure, undergoes a substantial elongation from the S_0 equilibrium structure. The whole relaxation process of the $S_3(2A')$ state from the Franck−Condon area to its C_s minimum is exothermic by 1.12 eV (from 5.67 to 4.55 eV, Figure 4). With this boat structure, the ground state (1A′) energy increases to 4.3 eV and the 1A″ state energy increases from 4.07 to 5.10 eV. As a consequence, the energy gaps between $S_0(1A')-S_1(2A')$ and $S_1(2A')-S_3(1A'')$ are substantially reduced to 0.22 and 0.55 eV, respectively (see Figure 4, left part). This result suggests that this out-of-plane relaxation pathway of the $S_3(2A')$ state into the $S_1(1A')$ state may be competitive with the in-plane mechanism of relaxation from the higher excited electronic states, which will be described in the next section.

3.3.4. Mechanism of Relaxation in C_{2v} Symmetry: S_1/S_2 Conical Intersection. We have observed that the excited states having a $\pi\pi^*$ character, $S_1(1B_2)$ and $S_3(2A_1)$, can undergo a fast relaxation process through a conical intersection with the ground state along out-of-plane coordinates. On the other hand, the $\sigma\pi^*$ states, $S_2(1A_2)$ and $S_4(1B_1)$, stay planar during optimization, keep the C_{2v} symmetry, and thus might be stable with respect to nonradiative decay. Hence, we have searched for other pathways with C_{2v} symmetry, which may lead to conical intersections between the $\sigma\pi^*$ states and the $\pi\pi^*$ states.

First, all four excited states have been optimized within the C_{2v} constraint. Here we took advantage of the fact that the four lowest excited states all belong to different irreducible representations of the C_{2v} symmetry group. Thus, each state could readily be optimized in its own symmetry block. The geometric parameters of the optimized structures of these four states (CC2/cc-pVDZ) are gathered in Table 1 and are compared with the C_{2v} structure of the S_0 state (MP2/cc-pVDZ). Closer inspection of this table reveals reveals that for the optimized geometries of both the $S_1(\pi\pi^*)$ and the $S_2(\sigma\pi^*)$ states the C2−C3 interatomic distance becomes significantly shorter (in comparison with the S_0 geometry) and the C2−C1−C3 bond angle decreases substantially. In contrast, in the case of the $S_3(\pi\pi^*)$ and $S_4(\sigma\pi^*)$ states, the C2−C3 distance is elongated in their minimum geometries and the C2−C1−C3 bond angle is increased. On the basis of this observation, the C2−C3 distance has been chosen as the driving coordinate to illustrate the interplay between the considered electronic states. The potential energy (PE) profiles calculated along the minimum energy paths for an elongation of the C2−C3 distance are presented in Figure 5. Full lines represent the PE profiles of reaction paths determined for each electronic state in C_{2v} symmetry. These profiles show how the system would initially respond when populated in a given state, because in-plane deformations are expected to occur on a shorter time scale than out-of-plane ones. The dashed lines represent the PE profiles of the other states calculated at the optimized geometry of a given state.

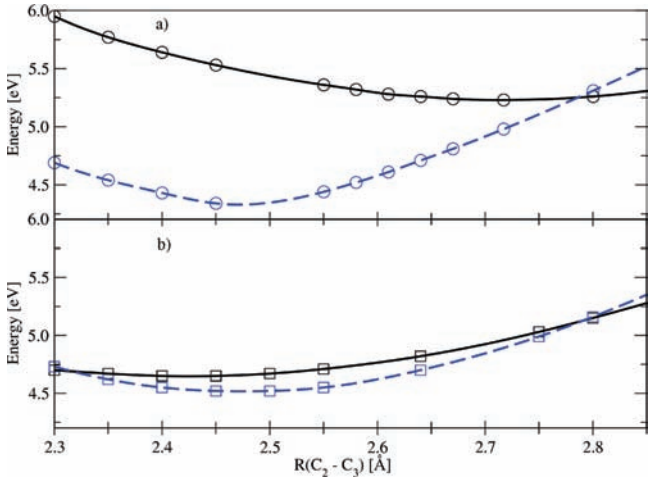

Figure 5. Potential energy (PE) profiles calculated at the CC2/cc-pVDZ level along the minimum energy paths for an elongation of C2−C3 distance in C_{2v} symmetry. (a) The full line represents the PE profile of the reaction path determined for the $S_4(1B_1, \pi\sigma^*)$ state; the dashed line represents the PE profile of the lower excited $S_1(1B_2, \pi\pi^*)$ state at the geometry of the $1B_1$ state. (b) The full line represents the PE profile of the reaction path determined for the $S_2(1A_2, \pi\sigma^*)$ state; the dashed line represents the PE profile of the lower excited $S_1(1B_2, \pi\pi^*)$ state at the geometry of the $1A_2$ state.

Such profiles are helpful to localize the crossings between the different electronic states and, consequently, to predict the geometry of conical intersections between them. For example, once the $1B_1(\sigma\pi^*)$ state is populated, the system relaxes along its adiabatic PE profile to reach its minimum geometry at the C2−C3 distance at 2.7 Å. At this minimum the energy of the $1B_2(\pi\pi^*)$ state is very close to the energy of the $1B_1$ state, indicating the presence of a conical intersection between these two states (Figure 5a). After a nonadiabatic transition at the $1B_1/1B_2$ conical intersection, the wavepacket can further relax on the $1B_2(\pi\pi^*)$ surface toward its intersection with the ground state. Similarly, it can be seen that the $1A_2(\sigma\pi^*)$ state at its equilibrium has a similar energy as the vertical energy of the $1B_2(\pi\pi^*)$ state calculated at the energy of the former state. Thus, the $1A_2$ state is expected to decay also into the $S_1(\pi\pi^*)$ surface quite readily (Figure 5b).

To validate the application of the CC2 method in predicting the minimum energy paths for this molecular ion, we have performed CASPT2 single-point calculations for the crucial points on the minimum energy paths of the B_1 and A_2 excited states presented in parts a and b of Figure 5, respectively, i.e., at the conical intersections. The agreement between the results of these two techniques (presented in Table S3 in the Supporting Information) is surprisingly good, suggesting that the contributions of double excitations for the proper description of the electronic structure of the considered excited states and their energetics are minor. The CASPT2 energies, calculated at the crossings of the A_2 state with the B_2 state (Figure 5b) occurring at 2.30 and 2.75 Å and at the crossing of the B_1 state with the B_2 state at 2.80 Å (Figure 5a) are systematically lower than the corresponding CC2 energies by 0.25−0.38 eV. Significantly, the CASPT2 technique confirms the degeneracy of the considered states at the respective crossing point geometries predicted by the CC2 method. Furthermore, the excitation energies ΔE_a for the B_2 and A_2 excited states calculated at the CASPT2/cc-pVDZ level, 3.50 and 4.36 eV, are only ca. 0.3 eV lower than the corresponding CC2 values of 3.82 and 4.64 eV, respectively (see Table S2 in Supporting Information).

3.4. Comparison to Experiment. The UV spectrum of isolated $C_6H_7^+$ has been recorded via photodissociation spectroscopy in an ion cyclotron resonance mass spectrometer (Figure 3a).[12,13] Within the investigated spectral range (235−400 nm, 3.10−5.28 eV), two absorption bands have been observed with band maxima at 330 and 245 nm (3.76 and 5.06 eV) and relative intensities of 4:1, respectively. Thus, by comparison with the present calculations, the 330 nm band can readily be assigned to excitation of $C_6H_7^+$ from the S_0 to the S_1 state. The calculated vertical transition energy of 4.07 eV (3.82 eV in C_{2v}) compares very favorably with the experimental band maximum of 3.76 eV. The interpretation of the second, less intense experimental band at 5.06 eV is less certain. The first option is an assignment to the optically forbidden S_2 state calculated at a vertical transition energy of 5.52 eV (4.65 eV relaxed in C_{2v}), which may become active via vibronic coupling. In this case, the optically allowed and intense S_3-S_0 transition calculated at a vertical transition energy of 5.67 eV (5.46 eV relaxed in C_{2v}) may have been outside of the spectral range investigated in the experimental spectrum. An alternative and more likely interpretation of the 245 nm band is in fact an assignment of the transition to the optically allowed S_3 state. The fact that the geometry of the S_3 state in the Franck−Condon region is very different from its minimum structure can explain the large difference between the higher-lying vertical transition energy and the adiabatic transition energy. Thus, the calculated vertical transition energy may overestimate the experimentally observed band center. As discussed in section 3.2, the CC2 level in general tends to somewhat overestimate the excitation energies, which may also partly account for the discrepancy between the experimental and calculated spectrum in Figure 3.

It is difficult to extract any information about the lifetime of the excited states from the experimental spectrum in Figure 3a. Several factors contribute to the widths of the experimental transitions observed at 3.76 and 5.06 eV (∼0.4 and 0.7 eV), including the limited spectral resolution of the monochromator employed ($\Delta\lambda = 10$ nm correspond to $\Delta E \sim 0.15$ at 4 eV), the unresolved (ro)vibrational structure arising from Franck−Condon progressions expected for the large geometry changes predicted by the present calculations, and possibly lifetime broadening. In any case, the width of 0.4 eV of the 330 nm band provides a lower limit to the lifetime of the S_1 state of 1.6 fs. Higher resolution UV spectra of cold $C_6H_7^+$ ions generated either in a molecular beam or in a cold ion trap and/or time-resolved spectroscopic experiments are required to extract more definitive information about the lifetime of the excited states. Such studies are currently under way.

4. Concluding Remarks

On the basis of ab initio calculations, we predict that none of the first four excited singlet states of protonated benzene will show any measurable fluorescence but will undergo a very fast nonradiative decay, probably on the femtosecond time scale. The $\pi\pi^*$ states (S_1 and S_3) will decay in a barrierless manner through a conical intersection with the ground state via out-of-plane deformations of the ring. The $\sigma\pi^*$ states (S_2 and S_4) will decay through a conical intersection with the $\pi\pi^*$ states via an in-plane ring deformation. It is then a challenge for the experimentalist to check this prediction! Corresponding experiments are under way.

Comparison of the relaxation pathways of protonated benzene ion ($C_6H_7^+$) with those of the isoelectronic neutral

benzene molecule (C_6H_6) reveals the significant effects of protonation on the photophysical properties of the aromatic molecule. Similar to $C_6H_7^+$, the relaxation pathway and the resulting nonradiative decay ("channel three")[79] of the S_1 state of C_6H_6 associated with the existence of a conical intersection was previously shown to proceed via an out-of-plane deformation toward a prefulvenic structure (chair). However, in contrast to $C_6H_7^+$, this process involves a barrier in the case of C_6H_6, implying that this relaxation channel opens only at an excess energy of about 3000 cm^{-1} in the S_1 state.[74,76,80] This excess energy is required to overcome the low-energy barrier in the S_1 state of C_6H_6 to its prefulvenic unstable form. Interestingly, protonation of C_6H_6 removes this barrier in the S_1 excited state, thus demonstrating that protonation of aromatic molecules can induce substantial modifications of their photophysical properties.

Acknowledgment. This work has been supported by research grants from the Interdisciplinary Center of Mathematical and Computer Modeling (ICM) of Warsaw University (Grant No. G29-11), the *Deutsche Forschungsgemeinschaft* (DO 729/2), the DAAD Procope program (D/0707510, 17832 NK), and the CNRS/PAN agreement (19502).

Supporting Information Available: Complete citations for refs 67 and 72, a figure showing potential energy profiles, and tables providing excitation energies, excited-state energies, and structural parameters. This information is available free of charge via the Internet at http://pubs.acs.org/.

References and Notes

(1) Kiendler, A.; Arnold, F. *Atmos. Environ.* **2002**, *36*, 2979–2984.
(2) Olah, G. A. *Acc. Chem. Res.* **1971**, *4*, 240.
(3) Smith, M. B.; March, J. *Advanced Organic Chemistry: Reactions, Mechanisms, and Structure*, 5th ed.; Wiley: New York, 2001.
(4) Weilmünster, P.; Keller, A.; Homann, K. H. *Combust. Flame* **1999**, *116*, 62–83.
(5) Snow, T.; Page, L. V.; Keheyan, Y.; Bierbaum, V. M. *Nature (London)* **1998**, *391*, 259.
(6) Lorenz, U. J.; Solca, N.; Lemaire, J.; Maitre, P.; Dopfer, O. *Angew. Chem., Int. Ed.* **2007**, *46*, 6714.
(7) Douberly, G. E.; Ricks, A. M.; Schleyer, P. V. R.; Duncan, M. A. *J. Phys. Chem. A* **2008**, *112*, 4869–4874.
(8) Sobolewski, A. L.; Domcke, W.; Dedonder-Lardeux, C.; Jouvet, C. *Phys. Chem. Chem. Phys.* **2002**, *4*, 1093–1100.
(9) Boyarkin, O. V.; Mercier, S. R.; Kamariotis, A.; Rizzo, T. R. *J. Am. Chem. Soc.* **2006**, *128*, 2816.
(10) Kang, H.; Dedonder-Lardeux, C.; Jouvet, C.; Gregoire, G.; Desfrancois, C.; Schermann, J. P.; Barat, M.; Fayeton, J. A. *J. Phys. Chem. A* **2005**, *109*, 2417–242.
(11) Solcà, N.; Dopfer, O. *Angew. Chem., Int. Ed.* **2002**, *41*, 3628.
(12) Freiser, B. S.; Beauchamp, J. L. *J. Am. Chem. Soc.* **1976**, *98*, 3136.
(13) Freiser, B. S.; Beauchamp, J. L. *J. Am. Chem. Soc.* **1977**, *99*, 3214.
(14) Solcà, N.; Dopfer, O. *J. Am. Chem. Soc.* **2003**, *125*, 1421.
(15) Solcà, N.; Dopfer, O. *J. Am. Chem. Soc.* **2004**, *126*, 1716.
(16) Solcà, N.; Dopfer, O. *Chem.—Eur. J.* **2003**, *9*, 3154.
(17) Solcà, N.; Dopfer, O. *Chem. Phys. Lett.* **2001**, *342*, 191.
(18) Andrei, H. S.; Solcà, N.; Dopfer, O. *ChemPhysChem* **2006**, *7*, 107–110.
(19) Talbot, F. O.; Tabarin, T.; Antoine, R.; Broyer, M.; Dugourd, P. *J. Chem. Phys.* **2005**, *122*.
(20) Solcà, N.; Dopfer, O. *ChemPhysChem* **2005**, *6*, 434.
(21) Solcà, N.; Dopfer, O. *J. Chem. Phys.* **2004**, *121*, 769.
(22) Solcà, N.; Dopfer, O. *J. Chem. Phys.* **2004**, *120*, 10470.
(23) Jones, W.; Boissel, P.; Chiavarino, B.; Crestoni, M. E.; Fornarini, S.; Lemaire, J.; Maitre, P. *Angew. Chem., Int. Ed.* **2003**, *42*, 2057.
(24) Dopfer, O.; Lemaire, J.; Maitre, P.; Crestoni, M. E.; Fornarini, S. *Int. J. Mass Spectrom.* **2006**, *249−250*, 149–154.
(25) Dopfer, O. *J. Phys. Org. Chem.* **2006**, *19*, 540–551.
(26) Dopfer, O.; Lemaire, J.; Maitre, P.; Crestoni, M. E.; Fornarini, S. *Int. J. Mass Spectrom.* **2007**, *267*, 43–53.
(27) Oomens, J.; von Helden, G.; Meijer, G. *J. Phys. Chem. A* **2004**, *108*, 8273.
(28) Oomens, J.; von Helden, G.; Meijer, G. *Int. J. Mass Spectrom.* **2006**, *249−250*, 199–205.
(29) Stearns, J. A.; Mercier, S.; Seaiby, C.; Guidi, M.; Boyarkin, O. V.; Rizzo, T. R. *J. Am. Chem. Soc.* **2007**, *129*, 11814–1182.
(30) Stearns, J. A.; Boyarkin, O. V.; Rizzo, T. R. *J. Am. Chem. Soc.* **2007**, *129*, 13820.
(31) Fujihara, A.; Matsumoto, H.; Shibata, Y.; Ishikawa, H.; Fuke, K. *J. Phys. Chem. A* **2008**, *112*, 1457–1463.
(32) Kang, H.; Dedonder-Lardeux, C.; Jouvet, C.; Martrenchard, S.; Gregoire, G.; Desfrancois, C.; Schermann, J. P.; Barat, M.; Fayeton, J. A. *Phys. Chem. Chem. Phys.* **2004**, *6*, 2628–263.
(33) Kang, H.; Jouvet, C.; Dedonder-Lardeux, C.; Martrenchard, S.; Gregoire, G.; Desfrancois, C.; Schermann, J. P.; Barat, M.; Fayeton, J. A. *Phys. Chem. Chem. Phys.* **2005**, *7*, 394–398.
(34) Nolting, D.; Schultz, T.; Hertel, I. V.; Weinkauf, R. *Phys. Chem. Chem. Phys.* **2006**, *8*, 5247–5254.
(35) Lucas, B.; Barat, M.; Fayeton, J. A.; Perot, M.; Jouvet, C.; Gregoire, G.; Nielsen, S. B. *J. Chem. Phys.* **2008**, *128*, 134313.
(36) Lepere, V.; Lucas, B.; Barat, M.; Fayeton, J. A.; Picard, V. J.; Jouvet, C.; Carcabal, P.; Nielsen, I.; Dedonder-Lardeux, C.; Gregoire, G.; Fujii, A. *J. Chem. Phys.* **2007**, *127*.
(37) Ahlrichs, R.; Bär, M.; Häser, M.; Horn, H.; Kölmel, C. *Chem. Phys. Lett.* **1989**, *162*, 165–169.
(38) Gregoire, G.; Jouvet, C.; Dedonder, C.; Sobolewski, A. L. *J. Am. Chem. Soc.* **2007**, *129*, 6223–6231.
(39) Gregoire, G.; Jouvet, C.; Dedonder, C.; Sobolewski, A. L. *Chem. Phys.* **2006**, *324*, 398–404.
(40) Marian, C.; Nolting, D.; Weinkauf, R. *Phys. Chem. Chem. Phys.* **2005**, *7*, 3306–3316.
(41) Glukhovtsev, M. N.; Pross, A.; Nicolaides, A.; Radom, L. *J. Chem. Soc., Chem. Commun.* **1995**, 2347.
(42) Maksic, Z. B.; Kovacevic, B.; Lesar, A. *Chem. Phys.* **2000**, *253*, 59.
(43) Sumathy, R.; Kryachko, E. S. *J. Phys. Chem. A* **2002**, *106*, 510, and references therein.
(44) Olah, G. A.; Staral, J. S.; Asencio, G.; Liang, G.; Forsyth, D. A.; Mateescu, G. D. *J. Am. Chem. Soc.* **1978**, *100*, 6299.
(45) Okami, Y.; Nanbu, N.; Okuda, S.; Hamanaka, S.; Ogawa, M. *Tetrahedron Lett.* **1972**, *51*, 5259.
(46) Xu, T.; Barich, D. H.; Torres, P. D.; Haw, J. F. *J. Am. Chem. Soc.* **1997**, *119*, 406.
(47) Reed, C. A.; Fackler, N. L. P.; Kim, K. C.; Stasko, D.; Evans, D. R.; Boyd, P. D. W.; Rickard, C. E. F. *J. Am. Chem. Soc.* **1999**, *121*, 631.
(48) Stasko, D.; Reed, C. A. *J. Am. Chem. Soc.* **2002**, *124*, 1148.
(49) Reed, C. A.; Kim, K. C.; Stoyanov, E. S.; Stasko, D.; Tham, F. S.; Mueller, L. J.; Boyd, P. D. W. *J. Am. Chem. Soc.* **2003**, *125*, 1796–1804.
(50) Perkampus, H. H.; Baumgarten, E. *Angew. Chem., Int. Ed. Engl.* **1964**, *3*, 776.
(51) Dopfer, O.; Solcà, N.; Lemaire, J.; Maitre, P.; Crestoni, M. E.; Fornarini, S. *J. Phys. Chem. A* **2005**, *109*, 7881.
(52) Muller, N.; Pickett, L. W.; Mulliken, R. S. *J. Am. Chem. Soc.* **1954**, *76*, 4770–4778.
(53) Dallinga, G.; Mackor, E. L.; Stuart, A. A. V. *Mol. Phys.* **1958**, *1*, 123–140.
(54) Kawashima, Y.; Nakayama, K.; Nakano, H.; Hirao, K. *Chem. Phys. Lett.* **1997**, *267*, 82–90.
(55) Salzner, U. *J. Chem. Theory Comput.* **2007**, *3*, 219–231.
(56) Salzner, U. *J. Chem. Theory Comput.* **2007**, *3*, 1143–1157.
(57) Weigend, F.; Häser, M. *Theor. Chem. Acc.* **1997**, *97*, 331–340.
(58) Moller, C.; Plesset, M. S. *Phys. Rev.* **1934**, *46*, 618.
(59) Bauernschmitt, R.; Ahlrichs, R. *J. Chem. Phys.* **1996**, *104*, 9047–9052.
(60) Bauernschmitt, R.; Ahlrichs, R. *Chem. Phys. Lett.* **1996**, *256*, 454–464.
(61) Christiansen, O.; Koch, H.; Jorgensen, P. *Chem. Phys. Lett.* **1995**, *243*, 409–418.
(62) Hättig, C.; Weigend, F. *J. Chem. Phys.* **2000**, *113*, 5154–5161.
(63) Köhn, A.; Hättig, C. *J. Chem. Phys.* **2003**, *119*, 5021–5036.
(64) Furche, F.; Rappoport, D. In *Computational Photochemistry*; Olivucci, M., Ed.; Elsevier: Amsterdam, 2005; Vol. 16.
(65) Werner, H. J. *Mol. Phys.* **1996**, *89*, 645–661.
(66) Celani, P.; Werner, H. J. *J. Chem. Phys.* **2000**, *112*, 5546–5557.
(67) MOLPRO is a package of ab initio programs written by Werner, H.-J. and Knowles, P. J. with contributions from Lindh, R., et al., version 2008.1.
(68) Roos, B. *Adv. Chem. Phys.* **1987**, *6*, 399.
(69) Chmura, B.; Rode, M. F.; Sobolewski, A. L.; Lapinski, L.; Nowak, M. J. *J. Phys. Chem. A* **2008**, *112*, 13655.
(70) Becke, A. D. *J. Chem. Phys.* **1993**, *98*, 5648–5652.
(71) Dunning, T. H. *J. Chem. Phys.* **1989**, *90*, 1007–1023.
(72) Frisch, M. J.; et al. *Gaussian 03, Revision C.02.*, Gaussian, Inc.: Pittsburgh, PA, 2004.

(73) Hattig, C.; Hald, K. *Phys. Chem. Chem. Phys.* **2002**, *4*, 2111–2118.
(74) Kato, S. *J. Chem. Phys.* **1988**, *88*, 3045–3056.
(75) Sobolewski, A. L.; Domcke, W. *Chem. Phys. Lett.* **1991**, *180*, 381–386.
(76) Sobolewski, A. L.; Woywod, C.; Domcke, W. *J. Chem. Phys.* **1993**, *98*, 5627–5641.
(77) Sobolewski, A. L.; Domcke, W. *Chem. Phys. Lett.* **1993**, *211*, 82–87.
(78) Sobolewski, A. L.; Czerminski, R. *Chem. Phys.* **1989**, *130*, 123–128.
(79) Callomon, J. H.; Parkin, J. E.; Lopezdel, R. *Chem. Phys. Lett.* **1972**, *13*, 125.
(80) Palmer, I. J.; Ragazos, I. N.; Bernardi, F.; Olivucci, M.; Robb, M. A. *J. Am. Chem. Soc.* **1993**, *115*, 673–682.

JP902729M